
Learning Multiple Networks via Supervised Tensor Decomposition

Anonymous Author(s)

Affiliation

Address

email

Abstract

We consider the problem of tensor decomposition with multiple side information available as interactive features. Such problems are common in neuroimaging, network modeling, and spatial-temporal analysis. We develop a new family of exponential tensor decomposition models and establish the theoretical accuracy guarantees. An efficient alternating optimization algorithm is further developed. Unlike earlier methods, our proposal handles a broad range of data types, including continuous, count, and binary observations, along with available features. We apply the method to diffusion tensor imaging data from human connectome project and identify the key brain connectivity patterns associated with available features. Our method will help the practitioners efficiently analyze tensor datasets in various areas. Toward this end, all data and code has been made available to the public.

1 Introduction

Higher-order tensors have received increased attention across science and engineering. While most tensor decomposition methods are developed for a single tensor observation, scientific studies often collect side information, in the form of node features and interactions thereof, together with the tensor data. Such data problems are common in neuroimaging, network analysis, and spatial-temporal modeling. A popular example is in neuroimaging (Zhou et al., 2013). The brain connectivity networks are collected from a sample of individuals, accompanied by individual characteristics such as age, gender, and diseases status (see Figure 1a). Another example is in network analysis (Berthet and Baldwin, 2020). Side information such as people’s demographic information and friendship types are often available. In both examples, scientists are interested in identifying the variation in the data tensor (e.g., brain connectivities, social community patterns) that is affected by available features. These seemingly different scenarios pose a common yet challenging problem for tensor data modeling.

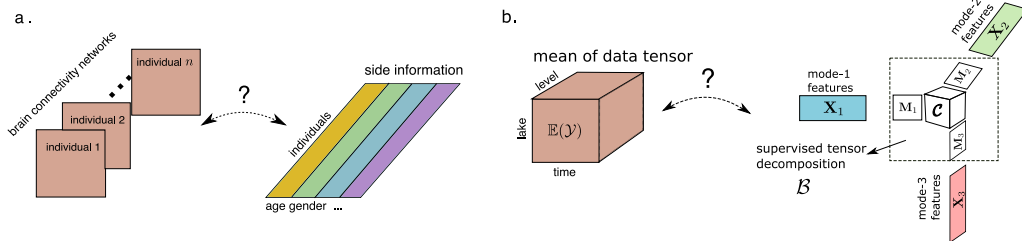


Figure 1: Examples of supervised tensor decomposition with interactive side information. (a) Network population model. (b) Spatio-temporal growth model.

In addition to the challenge of incorporating side information, many tensor datasets consist of non-Gaussian measurements. Classical tensor decomposition methods are based on minimizing the

26 Frobenius norm of deviation, leading to suboptimal predictions for binary- or count-valued response
 27 variables. A number of supervised tensor methods have been proposed (Narita et al., 2012; Zhao et al.,
 28 2012; Yu and Liu, 2016; Lock and Li, 2018). These methods often assume Gaussian distribution for
 29 the tensor entries, or impose random designs for the feature matrices, both of which are less suitable
 30 for applications of our interest. The gap between theory and practice means a great opportunity to
 31 modeling paradigms and better capture the complexity in tensor data.

32 **Our contribution.** This paper presents a general model and associated method for decomposing a
 33 data tensor whose entries are from exponential family with interactive side information. We formulate
 34 the learning task as a low-rank tensor regression problem, with tensor observation serving as the
 35 response, and the multiple side information as interactive features. We blend the modeling power of
 36 generalized linear model (GLM) and the exploratory capability of tensor dimension reduction in order
 37 to take the best out of both worlds. Our methods greatly improves the classical tensor decomposition,
 38 and we quantify the gain in prediction through numerical experiments and data applications.

39 **Notation.** We follow the tensor notation as in Kolda and Bader (2009). The multilinear mul-
 40 tiplication of a tensor $\mathcal{Y} \in \mathbb{R}^{d_1 \times \dots \times d_K}$ by matrices $\mathbf{X}_k = [\mathbf{x}_{i_k, j_k}^{(k)}] \in \mathbb{R}^{p_k \times d_k}$ is defined
 41 as $\mathcal{Y} \times \{\mathbf{X}_1, \dots, \mathbf{X}_K\} = [\sum_{i_1, \dots, i_K} y_{i_1, \dots, i_K} x_{j_1, i_1}^{(1)} \cdots x_{j_K, i_K}^{(K)}]$, which results in an order- K
 42 (p_1, \dots, p_K)-dimensional tensor. The inner product between two tensors of equal size is defined as
 43 $\langle \mathcal{Y}, \mathcal{Y}' \rangle = \sum_{i_1, \dots, i_K} y_{i_1, \dots, i_K} y'_{i_1, \dots, i_K}$. For ease of notation, we allow basic arithmetic operators
 44 (e.g., $+$, $-$) and univariate functions $f: \mathbb{R} \rightarrow \mathbb{R}$ to be applied to tensors in an element-wise manner.

45 2 Proposed models and motivating examples

46 Let $\mathcal{Y} = [y_{i_1, \dots, i_K}] \in \mathbb{R}^{d_1 \times \dots \times d_K}$ denote an order- K data tensor. Suppose the side information is
 47 available on each of the K modes. Let $\mathbf{X}_k = [\mathbf{x}_{i,j}] \in \mathbb{R}^{d_k \times p_k}$ denote the feature matrix on the mode
 48 $k \in [K]$, where $x_{i,j}$ denotes the j -th feature value for the i -th tensor entity, for $(i, j) \in [d_k] \times [p_k]$,
 49 $p_k \leq d_k$. We assume that, conditional on the features \mathbf{X}_k , the entries of tensor \mathcal{Y} are independent
 50 realizations from an exponential family distribution, and the conditional mean tensor admits the form

$$\begin{aligned} \mathbb{E}(\mathcal{Y} | \mathbf{X}_1, \dots, \mathbf{X}_K) &= f(\mathcal{C} \times \{\mathbf{X}_1 \mathbf{M}_1, \dots, \mathbf{X}_K \mathbf{M}_K\}), \\ \text{with } \mathbf{M}_k^T \mathbf{M}_k &= \mathbf{I}_{r_k}, \quad \mathbf{M}_k \in \mathbb{R}^{p_k \times r_k} \quad \text{for all } k = 1, \dots, K. \end{aligned} \quad (1)$$

51 where $\mathcal{C} \in \mathbb{R}^{r_1 \times \dots \times r_K}$ is a full-rank core tensor, and $\mathbf{M}_k \in \mathbb{R}^{p_k \times r_k}$ are factor matrices consisting
 52 of orthonormal columns, where $r_k \leq p_k$ for all $k \in [K]$, $f(\cdot)$ is a known link function whose form
 53 depending on the data type of \mathcal{Y} . Common choices of link functions include identity link for Gaussian
 54 distribution, logistic link for Bernoulli distribution, and $\exp(\cdot)$ link for Poisson distribution.

55 Figure 1b provides a schematic illustration of our model. The features \mathbf{X}_k affect the distribution of
 56 tensor entries in \mathcal{Y} through the form $\mathbf{X}_k \mathbf{M}_k$, which are r_k linear combinations of features on mode k .
 57 The core tensor \mathcal{C} collects the interaction effects between sufficient features across K modes, which
 58 links the conditional mean to the feature spaces, and thereby allows the identification of variations in
 59 the tensor data attributable to the side information. Our goal is to find \mathbf{M}_k and the corresponding \mathcal{C} ,
 60 thereby allowing us to reveal the relationship between side information \mathbf{X}_k and the observed tensor
 61 \mathcal{Y} . Note that \mathbf{M}_k and \mathcal{C} are identifiable only up to orthonormal transformations.

62 We give two examples of supervised tensor decomposition models (1) that arise in practice.

63 **Example 1** (Spatio-temporal growth model). The growth curve model (Srivastava et al., 2008) was
 64 originally proposed as an example of bilinear model for matrix data, and we extend it to higher-order
 65 cases. Let $\mathcal{Y} = [y_{ijk}] \in \mathbb{R}^{d \times m \times n}$ denote the pH measurements of d lakes at m levels of depth
 66 and for n time points. Suppose the sampled lakes belong to q types, with p lakes in each type. Let
 67 $\{\ell_j\}_{j \in [m]}$ denote the sampled depth levels and $\{t_k\}_{k \in [n]}$ the time points. Assume that the expected
 68 pH trend in depth is a polynomial of order at most r and that the expected trend in time is a polynomial
 69 of order s . Then, the conditional mean model for the spatio-temporal growth is a special case of our
 70 model (1), where $\mathbf{X}_1 = \text{blockdiag}\{\mathbf{1}_q, \dots, \mathbf{1}_q\} \in \{0, 1\}^{d \times p}$ is the design matrix for lake types,

$$\mathbf{X}_2 = \begin{pmatrix} 1 & \ell_1 & \cdots & \ell_1^r \\ 1 & \ell_2 & \cdots & \ell_2^r \\ \vdots & \vdots & \ddots & \vdots \\ 1 & \ell_m & \cdots & \ell_m^r \end{pmatrix}, \quad \mathbf{X}_3 = \begin{pmatrix} 1 & t_1 & \cdots & t_1^s \\ 1 & t_2 & \cdots & t_2^s \\ \vdots & \vdots & \ddots & \vdots \\ 1 & t_n & \cdots & t_n^s \end{pmatrix}$$

71 are the design matrices for spatial and temporal effects, respectively. The spatial-temporal mode has
 72 covariates available on each of the three modes.

73 **Example 2** (Network population model). Network response model is recently developed in the
 74 context of neuroimaging analysis. The goal is to study the relationship between network-valued
 75 response and the individual covariates. Suppose we observe n i.i.d. observations $\{(\mathbf{Y}_i, \mathbf{x}_i) : i = 1, \dots, n\}$, where $\mathbf{Y}_i \in \{0, 1\}^{d \times d}$ is the brain connectivity network on the i -th individual, and
 76 $\mathbf{x}_i \in \mathbb{R}^p$ is the individual covariate such as age, gender, cognition, etc. The network-response
 77 model (Rabusseau and Kadri, 2016) has the form

$$\text{logit}(\mathbb{E}(\mathbf{Y}_i | \mathbf{x}_i)) = \mathcal{B} \times_3 \mathbf{x}_i, \quad \text{for } i = 1, \dots, n \quad (2)$$

79 where $\mathcal{B} \in \mathbb{R}^{d \times d \times p}$ is the coefficient tensor of interest. The model (2) is also a special case of our
 80 tensor-response model, with covariates on the last mode of the tensor.

81 3 Estimation algorithms

82 We develop a likelihood-based procedure to estimate \mathcal{C} and \mathbf{M}_k in (1). Ignoring constants that do not
 83 depend on Θ , the quasi log-likelihood of (1) is equal to

$$\mathcal{L}_{\mathcal{Y}}(\mathcal{C}, \mathbf{M}_1, \dots, \mathbf{M}_K) = \langle \mathcal{Y}, \Theta \rangle - \sum_{i_1, \dots, i_K} b(\theta_{i_1, \dots, i_K}) \text{ with } \Theta = \mathcal{C} \times \{\mathbf{M}_1 \mathbf{X}_1, \dots, \mathbf{M}_K \mathbf{X}_K\},$$

84 where $b(\theta) = \theta^2/2$ for Gaussian response, $b(\theta) = \exp(\theta)$ for Poisson response, and $b(\theta) =$
 85 $\log(1 + \exp(\theta))$ for Bernoulli response. We propose a constrained maximum quasi-likelihood
 86 estimator (M-estimator),

$$(\hat{\mathcal{C}}, \hat{\mathbf{M}}_1, \dots, \hat{\mathbf{M}}_K) = \arg \max_{(\mathcal{C}, \mathbf{M}_1, \dots, \mathbf{M}_K) \in \mathcal{P}} \mathcal{L}_{\mathcal{Y}}(\mathcal{C}, \mathbf{M}_1, \dots, \mathbf{M}_K), \quad (3)$$

87 where parameter space $\mathcal{P} = \left\{ (\mathcal{C}, \mathbf{M}_1, \dots, \mathbf{M}_K) \mid \mathbf{M}_k^T \mathbf{M}_k = \mathbf{I}_{r_k}, \|\Theta(\mathcal{C}, \mathbf{M}_1, \dots, \mathbf{M}_K)\|_\infty \leq \alpha \right\}.$

88 The decision variables in the objective function (3) consist of $K + 1$ blocks of variables, one for the
 89 core tensor \mathcal{C} and K for the factor matrices \mathbf{M}_k . We notice that, if any K out of the $K + 1$ blocks of
 90 variables are known, then the optimization reduces to a simple GLM with respect to the last block
 91 of variables. This observation leads to an iterative updating scheme for one block at a time while
 92 keeping others fixed. A simplified version of the algorithm is described in Algorithm 1.

Algorithm 1 Supervised Tensor Decomposition with Interactive Side Information (Simplified)

Input: Response tensor $\mathcal{Y} \in \mathbb{R}^{d_1 \times \dots \times d_K}$, feature matrices $\mathbf{X}_k \in \mathbb{R}^{d_k \times p_k}$ for $k = 1, \dots, K$, target
 Tucker rank $\mathbf{r} = (r_1, \dots, r_K)$, link function f , maximum norm bound α

Output: Estimated core tensor $\hat{\mathcal{C}} \in \mathbb{R}^{r_1 \times \dots \times r_K}$ and factor matrices $\hat{\mathbf{M}}_k \in \mathbb{R}^{p_k \times r_k}$.

1: Random initialization of the core tensor \mathcal{C} and factor matrices \mathbf{M}_k .

2: **while** Do until convergence **do**

3: Obtain $\tilde{\mathbf{M}}_k \in \mathbb{R}^{p_k \times r_k}$ by a GLM. Orthogonalize $\tilde{\mathbf{M}}_k$ by QR factorization, for $k \in [K]$.

4: Update the core tensor \mathcal{C} by solving a GLM. Rescale the core tensor \mathcal{C} such that $\|\mathcal{C}\|_{\max} \leq \alpha$.

5: **end while**

93 We provide the accuracy guarantee for the proposed M-estimator (3) by leveraging recent development
 94 in random tensor theory and high-dimensional statistics.

95 **Theorem 3.1** (Convergence). Let $(\hat{\mathcal{C}}, \hat{\mathbf{M}}_1, \dots, \hat{\mathbf{M}}_K)$ be the M-estimator in (3) and $\hat{\mathcal{B}} = \hat{\mathcal{C}} \times \hat{\mathbf{M}}_1 \times \dots \times \hat{\mathbf{M}}_K$. Define $r_{\text{total}} = \prod_k r_k$ and $r_{\max} = \max_k r_k$. Under mild technical assumptions, there
 96 exist two positive constants $C_1, C_2 > 0$, such that, with probability at least $1 - \exp(-C_1 \sum_k p_k)$,

$$\|\mathcal{B}_{\text{true}} - \hat{\mathcal{B}}\|_F^2 \leq \frac{C_2 r_{\text{total}} \sum_k p_k}{r_{\max} \prod_k d_k}, \quad \text{and} \quad \sin^2 \Theta(\mathbf{M}_{k,\text{true}}, \hat{\mathbf{M}}_k) \leq \frac{C_2 r_{\text{total}}}{r_{\max} \sigma_{\min}^2(\text{Unfold}_k(\mathcal{C}_{\text{true}})) \prod_k d_k} \frac{\sum_k p_k}{\prod_k d_k},$$

98 where $\sin \Theta(\mathbf{M}_{k,\text{true}}, \hat{\mathbf{M}}_k) = \|\mathbf{M}_{k,\text{true}}^T \hat{\mathbf{M}}_k^\perp\|_\sigma$ is the angle distance between column spaces.

99 Theorem 3.1 implies that the estimation has a convergence rate $\mathcal{O}(d^{-(K-1)})$ in the special case when
 100 tensor dimensions are equal on each of the modes, i.e., $d_k = d$ for all $k \in [K]$, and feature dimension
 101 grows with tensor dimension, $p_k = \gamma d$, $\gamma \in [0, 1]$, for $k \in [K]$. The convergence of our estimation
 102 becomes especially favorable as the order of tensor data increases.

103 **4 Numerical experiments**

104 We compare our supervised tensor decomposition (**STD**) with three other supervised tensor methods:
105 Higher-order low-rank regression (**HOLRR** Rabusseau and Kadri (2016)), Higher-order partial least
106 square (**HOPLS** Zhao et al. (2012)) and Subsampled tensor projected gradient (**TPG** Yu and Liu
107 (2016)). Figure 2 shows that **STD** outperforms others, especially in the low-signal, high-rank setting.
108 As the number of informative modes (i.e., modes with available features) increases, the **STD** exhibits
109 a substantial reduction in error whereas others remain unchanged (Figure 2b). This showcases the
110 benefit of incorporation of multiple features. The accuracy gain in Figure 2 demonstrates the benefit
111 of alternating algorithm – incorporation of informative modes also improves the estimation in the
112 non-informative modes.

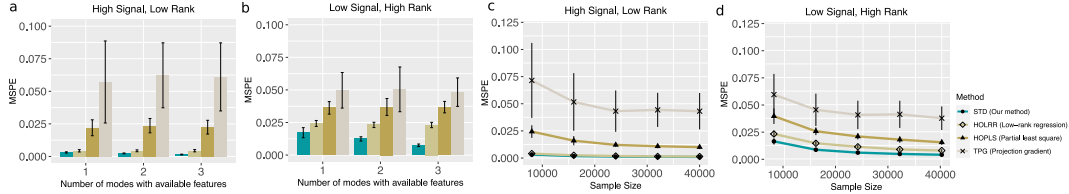


Figure 2: Comparison between different tensor methods. Panels (a) and (b) plot mean squared prediction error (MSPE) versus the number of modes with available features. Panels (c) and (d) plot MSPE versus the effective sample size d^2 . We consider rank $r = (3, 3, 3)$ (low) vs $(4, 5, 6)$ (high), and signal $\alpha = 3$ (low) vs. 6 (high).

113 We then apply our method to brain structural connectivity networks from Human Connectome Project
114 (HCP) (Geddes, 2016). The dataset consists of 136 brain structural networks, one for each individual.
115 Each brain network is represented as a 68-by-68 binary matrix, where the entries encode the presence
116 or absence of fiber connections between the 68 brain regions. We consider four individual features:
117 gender (65 females vs. 71 males), age 22-25 ($n = 35$), age 26-30 ($n = 58$), and age 31+ ($n = 43$).
118 The goal is to identify the connection edges that are affected by individual features.

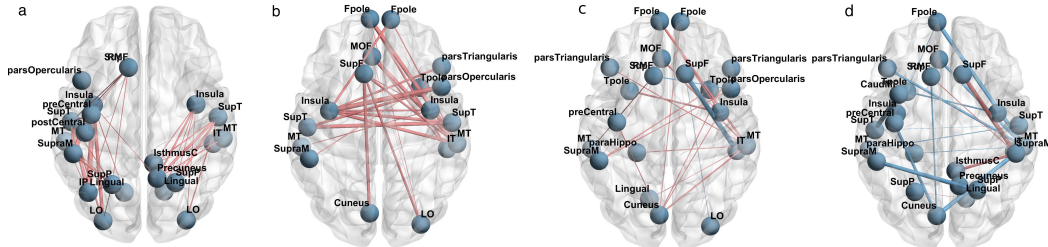


Figure 3: Top edges with large effects. (a) Global effect; (b) Female effect; (c) Age 22-25; (d) Age 31+. Red (blue) edges represent positive (negative) effects. Edge-widths are proportional to the magnitudes of effect sizes.

119 We perform the supervised tensor decomposition to the HCP data. The BIC selection suggests a
120 rank $r = (10, 10, 4)$ with quasi log-likelihood $\mathcal{L}_Y = -174654.7$. Figure 3 shows the top edges with
121 high effect size, overlaid on the Desikan atlas brain template (Desikan et al., 2006). We find that the
122 global connection exhibits clear spatial separation, and that the nodes within each hemisphere are
123 more densely connected with each other (Figure 3a). In particular, the superior-temporal (*SupT*),
124 middle-temporal (*MT*) and Insula are the top three popular nodes in the network. Interestingly, female
125 brains display higher inter-hemispheric connectivity, especially in the frontal, parietal and temporal
126 lobes (Figure 3b). This is in agreement with a recent study showing that female brains are optimized
127 for inter-hemispheric communication (Ingallalikar et al., 2014). We find several edges with declined
128 connection in the group Age 31+. Those edges involve Frontal-pole (*Fpole*), superior-frontal (*SupF*)
129 and Cuneus nodes. Our results highlight the importance of Frontal-pole region, and the detected
130 decline further suggests the age effects to brain connections.

131 **5 Conclusion**

132 We have developed a supervised tensor decomposition method with side information on multiple
133 modes. The empirical results demonstrate the improved interpretability and accuracy over previous
134 approaches. Applications to the brain connection data yield conclusions with sensible interpretations,
135 suggesting the practical utility of the proposed approach.

136 **Broader Impact**

137 Our supervised tensor decomposition method is widely applicable to network analysis, dyadic data
138 analysis, spatial-temporal model, and recommendation systems. We have shown the improved
139 predictive power and enhanced interpretability by incorporating the interactive side information in
140 tensor decomposition method. The application to the brain connection dataset yields conclusions with
141 sensible interpretations, suggesting the practical utility of the proposed approach. Tensor learning is a
142 clear challenge for further research. We believe that our model enriches the research of tensor-based
143 learning and is a powerful tool to boost scientific discoveries in various fields. We hope the work
144 opens up new inquiry that allows more machine learning researchers to contribute to this field.

145 **References**

- 146 Berthet, Q. and Baldin, N. (2020). Statistical and computational rates in graph logistic regression.
147 *Proceedings of the Twenty Third International Conference on Artificial Intelligence and Statistics*,
148 108:2719–2730.
- 149 Desikan, R. S., Ségonne, F., Fischl, B., Quinn, B. T., Dickerson, B. C., Blacker, D., Buckner,
150 R. L., Dale, A. M., Maguire, R. P., Hyman, B. T., et al. (2006). An automated labeling system
151 for subdividing the human cerebral cortex on MRI scans into gyral based regions of interest.
152 *Neuroimage*, 31(3):968–980.
- 153 Geddes, L. (2016). Human brain mapped in unprecedented detail. *Nature*.
- 154 Ingallalikar, M., Smith, A., Parker, D., Satterthwaite, T. D., Elliott, M. A., Ruparel, K., Hakonarson,
155 H., Gur, R. E., Gur, R. C., and Verma, R. (2014). Sex differences in the structural connectome of
156 the human brain. *Proceedings of the National Academy of Sciences*, 111(2):823–828.
- 157 Kolda, T. G. and Bader, B. W. (2009). Tensor decompositions and applications. *SIAM review*,
158 51(3):455–500.
- 159 Lock, E. F. and Li, G. (2018). Supervised multiway factorization. *Electronic journal of statistics*,
160 12(1):1150.
- 161 Narita, A., Hayashi, K., Tomioka, R., and Kashima, H. (2012). Tensor factorization using auxiliary
162 information. *Data Mining and Knowledge Discovery*, 25(2):298–324.
- 163 Rabusseau, G. and Kadri, H. (2016). Low-rank regression with tensor responses. In *Advances in
164 Neural Information Processing Systems*, pages 1867–1875.
- 165 Srivastava, M. S., von Rosen, T., and Von Rosen, D. (2008). Models with a kronecker product
166 covariance structure: estimation and testing. *Mathematical Methods of Statistics*, 17(4):357–370.
- 167 Yu, R. and Liu, Y. (2016). Learning from multiway data: Simple and efficient tensor regression. In
168 *International Conference on Machine Learning*, pages 373–381.
- 169 Zhao, Q., Caiafa, C. F., Mandic, D. P., Chao, Z. C., Nagasaka, Y., Fujii, N., Zhang, L., and Cichocki,
170 A. (2012). Higher order partial least squares (HOPLS): a generalized multilinear regression method.
171 *IEEE transactions on pattern analysis and machine intelligence*, 35(7):1660–1673.
- 172 Zhou, H., Li, L., and Zhu, H. (2013). Tensor regression with applications in neuroimaging data
173 analysis. *Journal of the American Statistical Association*, 108(502):540–552.